NONDESTRUCTIVE EVALUATION OF REINFORCED CONCRETE STRUCTURES AFFECTED BY ASR

Kerry Kreitman[1,*], Eric Giannini[1], Zachary Webb[1], Kevin J. Folliard[1], Oguzhan Bayrak[1], Jinying Zhu[1]

[1]The University of Texas at Austin, Austin, Texas, USA

Abstract

The deterioration of concrete structures by alkali-silica reaction (ASR) and delayed ettringite formation (DEF), which causes expansion and cracking similar to ASR, has been a worldwide problem in recent decades. A great deal of research into the causes and mechanisms of the deterioration has helped to prevent the formation of ASR and DEF in new construction, but the evaluation and maintenance of existing structures remains a problem. The goal of this research is to investigate the use of several nondestructive testing (NDT) methods to evaluate the level of deterioration in a structural element.

Keywords: Alkali-silica reaction, delayed ettringite formation, non-destructive testing

1 INTRODUCTION

Alkali-silica reaction (ASR) is a chemical process that deteriorates concrete by causing bulk expansion, extensive internal microcracking, and surface cracking. While a significant amount of ASR research has been completed in the past few decades, the evaluation and maintenance of in-service structures affected by ASR, with respect to serviceability and strength of the elements, is an area that still requires investigation. In particular, the actual behavior of large-scale reinforced concrete structures during load tests is not well predicted by the mechanical properties of concrete cores or unreinforced laboratory specimens. While it has widely been observed that the compressive strength, tensile strength, and elastic modulus of concrete are reduced by ASR [1,2], several researchers have found that the strength of reinforced elements is not significantly reduced by ASR deterioration [3-8]. This is particularly true for large scale laboratory specimens and field structures [9-13]. The reinforcement cage restrains the concrete expansions, effectively "prestressing" and confining the deteriorated concrete to maintain the structural integrity.

The goal of this research was to investigate the use of several nondestructive testing (NDT) methods for use in the evaluation of reinforced concrete structures affected by ASR [14]. While it was unlikely that a single NDT method would provide all of the information desired, this project investigated how NDT could supplement the existing testing and monitoring protocols, which focus on visual inspection and tests on drilled cores. To examine the potential for several NDT methods to evaluate ASR deterioration in structures, two large "reactive" beams were fabricated and conditioned to encourage accelerated deterioration. A third control, or "nonreactive", beam was also constructed. Over the monitoring period of about one year, expansions of these specimens were measured and four NDT methods were performed as deterioration progressed: ultrasonic pulse velocity (UPV), impact echo, spectral analysis of surface waves (SASW), and surface wave transmission (SWT). Additionally, small prism samples were cast with each of the three beam specimens and stored in a conditioning environment that encouraged rapid deterioration. Expansions of these prism samples were measured and the resonant frequency NDT method was performed throughout the

* Correspondence to: kerry.kreitman@utexas.edu

monitoring period. Observing trends in the correlation between the NDT measurements and the level of expansion led to conclusions regarding which NDT methods are most useful for evaluating the deterioration.

2 EXPERIMENTAL PROGRAM

2.1 Test Specimens

The beams were designed as near-full scale representations of bent caps found in the state of Texas. The geometry and reinforcement layout is depicted in Figure 1. Note that the beams were fabricated and stored with the tension steel at the top of the cross section, as future structural testing will be performed in this orientation (i.e. load applied from the bottom). Each specimen was approximately 8.4 m long with a 533 x 1067 mm cross section. Longitudinal reinforcement consisted of equal tension and compression bars for a flexural reinforcement ratio of 0.88%. Additional longitudinal bars were placed on the side faces to control cracking over the depth. Minimal transverse reinforcement was provided for a shear reinforcement ratio of 0.15% in the middle test region and of 0.31% in the outer test region. All steel had a yield stress of 425 MPa.

One of the most reactive aggregates in the state, Jobe-Newman sand from El Paso, Texas, was used to induce accelerated ASR deterioration in the reactive specimens. A total alkali content of 5.2 kg/m^3 was achieved through the use of high-alkali Type III cement and the addition of sodium hydroxide. A nonreactive river sand and low-alkali Type I cement was used in the fabrication of the nonreactive specimen, with no sodium hydroxide added. The total alkali content of the nonreactive specimen was only 2.0 kg/m^3. The water-cement ratio for all specimens was 0.57. Refer to Table 1 for details of both concrete mixtures.

In addition to promoting accelerated ASR deterioration by using reactive materials, delayed ettringite formation (DEF) was induced in the beam specimens. DEF is another chemical process which causes expansion and cracking similar to ASR in concrete experiencing high sustained curing temperatures (greater than 70°C) [15]. This study included both ASR and DEF because the two deterioration mechanisms are often found together in Texas. The reactive specimens were cured at high temperatures to induce DEF.

Eight small, unreinforced prism samples (76 x 76 x 286 mm) were also cast with each of the large specimens. These samples were "match cured" in an oven to approximate the curing temperature of the beams. Four of the prism samples from each beam were used for expansion monitoring while the other four were used for NDT.

2.2 Conditioning Program

The beams were stored outdoors in a warm climate to facilitate rapid deterioration. Additionally, a watering system was implemented by running soaker hoses along the length of each specimen. These hoses evenly provided moisture to all portions of the test regions during 12-minute overnight watering cycles. The specimens were wrapped in curing tarps to trap in the moisture during the day (see Figure 2).

To replicate field conditions as closely as possible, typical field-level dead load stresses were induced in the beams. This was accomplished by clamping each specimen against a steel reaction beam (W14x132) using tensioned steel rods. This is also depicted in the photograph in Figure 2.

The prism samples were conditioned according to ASTM C1293 [16]. This standard requires storage above water in plastic pails at 38°C starting 24 hours after casting. The samples were only removed from this environment during the specified monitoring intervals of 7 days, 14 days, and 1, 2, 3, 6, 9, and 12 months.

2.3 Expansion Monitoring

The level of deterioration was quantified by measuring the ASR/DEF-induced expansions of the beams at several locations in the longitudinal and vertical directions. Mechanical measurements of the core concrete expansions were taken using an extensometer (610 mm gauge length) to measure the distance

between stainless steel rods placed through the width of the specimens (533 mm dimension). Similarly, steel strains were measured using stainless steel studs welded to the longitudinal and transverse reinforcement. The rods and studs were isolated from the cover concrete using expandable foam surrounded by PVC pipe.

The length change of the prism samples was monitored according to ASTM C1293 [16].

2.4 Nondestructive Testing

The NDT methods of ultrasonic pulse velocity (UPV), impact echo, spectral analysis of surface waves (SASW), and surface wave transmission (SWT) were performed on the beam specimens as deterioration progressed. Additionally, the resonant frequency NDT method was performed on the prism samples.

To measure the compression wave velocity through the concrete, UPV testing was performed with a Germann Instruments PUNDIT 7 test system. 100 V pulses were imparted through the specimens at a pulse repetition frequency of 100 kHz using 54 kHz transducers and a water based couplant. The procedures of ASTM C597 were followed [17]. Measurements were taken at several locations in the middle and outer test regions (8 horizontally through the cross section at three different heights and 4 vertically through the cross section in each test region). All measurements were averaged together for each direction in each test region.

Impact echo testing was performed according to ASTM C1383 with a Germann Instruments DOCtor receiver and a 10 mm diameter ball-peen hammer [18]. Each signal was collected through an 8-bit National Instruments (NI) digitizer using a LabVIEW program, and analyzed using MATLAB. A sampling frequency of 100 kHz and a signal duration of 10 ms yielded a frequency resolution of 100 Hz. Measurements were taken near mid-depth on both side faces of the specimens. The compression wave velocity was computed from the peak frequency in the spectrum and the thickness of the element [19].

The two surface wave methods (SASW and SWT) involve the same test setup and data collection, but different analyses. After impact by a 13 mm steel ball, the signals were received by two non-contact sensors insulated from ambient noise. The use of non-contact sensors eliminates coupling problems and helps to speed up the testing process [20]. These sensors were PCB microphones with frequency sensitivity range of 4 Hz to 80 kHz. A PCB signal conditioner, an 8-bit NI digitizer, and a LabVIEW program were used to collect the data, which was then analyzed using MATLAB. A sampling frequency of 1 MHz was used to collect a 5 ms signal from each receiver. Testing was done at 5 locations in the vertical and horizontal directions on each side face of the specimens. Through frequency domain analysis, the surface wave velocity (SASW method) and fraction of energy transmitted (SWT method) between the receivers was computed [20,21].

Resonant frequency testing was performed on the small prism samples according to ASTM C215 [22]. A highly sensitive PCB accelerometer with a bandwidth of 0.5 Hz to 10 kHz was used to monitor the surface motion after an impact by an 11 mm steel ball. A PCB signal conditioner and an 8-bit NI digitizer were used to transmit data to a LabVIEW program for analysis. Testing was performed in both the longitudinal and transverse modes of free vibration. The dynamic elastic modulus was computed from the fundamental resonant frequencies, the mass, and the geometry [22].

3 RESULTS

3.1 Beam Specimen Expansions

Plots of the beam specimen expansions over the course of the monitoring period are shown in Figure 3. Each line represents the average expansion in a particular direction and test region for each specimen, including both the core concrete expansions and the steel strains. While individual measurements deviated from the average up to 0.1% expansion, the average value tended to lie near the center of the data spread.

From the results, it is obvious that the nonreactive specimen has not expanded. The most rapid expansion in each reactive specimen was attained in the vertical direction in the middle test region, where

maximum expansions of 0.56% and 0.94% were observed in the first and second reactive specimens, respectively. These values are approximately 2.3 and 3.8 times the yield strain of the reinforcement. The average longitudinal expansion over the entire beam tended to level off around 0.13-0.15% expansion, or 0.5-0.6 times the yield strain of the reinforcement, in both reactive specimens.

3.2 Beam Specimen NDT

The variation in the compression wave velocity from UPV and impact echo testing is depicted in Figures 4 and 5, respectively. Each point represents the average velocity from several measurements in one direction in a test region. The velocities measured in different directions by both methods yielded similar trends. A rapid drop in velocity occurred initially at low levels of expansion. As deterioration progressed, the decreasing slope became shallower and the velocity became less sensitive to the increasing expansion. In the first reactive specimen, the velocity leveled off to a relatively constant value at higher levels of expansion, while the velocity continued to decrease slightly as expansion increases in the second reactive specimen. The compression wave velocity in the nonreactive specimen fluctuated up and down in a range of about 3% change over the monitoring period. In contrast, a loss of 14-17% was observed in the velocity of the two reactive specimens.

Results from the SASW testing are presented in Figure 6, which shows the variation of the measured surface wave velocity as a function of the deterioration. After a rapid initial drop in the velocity, the data points were very scattered and did not indicate clear trends as expansion increased. There is also a distinct difference between the data taken in the longitudinal direction (black points) and that taken in the vertical direction (grey points), as the longitudinal velocities were consistently higher than the velocities in the vertical direction. The surface wave velocity in the nonreactive specimen fluctuated 8% over the monitoring period.

Figure 7 shows the variation of the measured surface wave energy transmission with expansion from SWT testing. Unlike the other methods, the energy transmission remained relatively constant and did not seem to be a function of the level of deterioration. The variation of the energy transmission in the nonreactive specimen fluctuated around 8% during the monitoring period.

3.3 Prism Samples

The measured expansions of the prism samples are presented in Figure 8. Each line in this figure represents the average expansion of four prism samples cast with each beam specimen. As with the beam specimens, the most rapid expansion was observed in the prism samples corresponding to the second reactive specimen. Maximum free expansions of the unreinforced prism samples were comparable to that of the reinforced beam specimens over a similar period of time, with maximum expansions of 0.60% and 0.85% measured in the prisms corresponding to the first and second reactive beam specimens, respectively. Additionally, the nonreactive prism exhibited essentially no expansion over the monitoring period.

Figure 9 shows the results from the resonant frequency testing, as plots of the variation of the average computed dynamic elastic modulus with prism expansion for both the longitudinal and transverse modes of vibration. Note that testing was started late for the prisms corresponding to the first reactive beam specimen so data points at low levels of expansion are not available for those prisms. The trends are very similar between the two vibrational modes, and the modulus calculated from the fundamental longitudinal resonant frequency was generally slightly higher than that in the transverse mode. The trends are comparable to those of the UPV and impact echo testing, with a rapid initial drop in modulus which leveled off as expansion increased. The modulus of the nonreactive prisms fluctuated about 2% over the monitoring period, compared to the 17-18% reduction in modulus observed in the reactive prism samples.

4 DISCUSSION

4.1 Beam Specimen Expansions

The nonreactive beam specimen did not exhibit any expansive tendencies, indicating that it is a sound, undamaged control specimen with no deterioration. As expected in the reactive specimens, more rapid expansion was observed in more lightly reinforced locations (i.e. the vertical direction in the middle test region). However, the relationship between reinforcement ratio and rate of expansion is nonlinear, making it difficult to predict expansion where it is not directly measured.

The main difference between the two reactive specimens was the curing temperature. The second reactive specimen sustained temperatures around 77°C for at least 12 hours during curing, while the first reactive specimen reached a maximum of around 70°C, but did not sustain this temperature for a significant period of time (recall that sustained curing temperatures greater than 70°C are required to induce DEF). Although a petrographic evaluation has yet to be performed, it is hypothesized that the second reactive specimen experienced deterioration from both ASR and DEF, while the first reactive specimen had only ASR deterioration. This explains the discrepancy in the expansion rate between the two reactive beams.

4.2 Beam Specimen NDT

Very similar results were obtained for the compression wave velocity using both the UPV and impact echo methods. This implies that either method can be used interchangeably, depending on the situation.

Although larger expansions are associated with lower velocities, all UPV and impact echo trends indicate that as expansion increases, velocity is less sensitive to deterioration. Most researchers believe this is because ASR gel fills the cracks, limiting the velocity reduction because the waves travel faster through the gel than through the air [23]. The results presented here uphold this theory, as the velocity in the first reactive specimen (likely having only ASR deterioration) levels off at higher expansions. One possible explanation for the slow, but continued, decrease of the velocity in the second reactive specimen at higher levels of expansion is that the additional cracks resulting from DEF (which does not produce gel) are not filled with ASR gel.

The results from the surface wave testing (SASW and SWT) yielded unclear trends. The scatter of the data points in the SASW results indicates that the method is sensitive to factors other than ASR/DEF. Additionally, the discrepancy between measurements in the longitudinal and vertical directions verifies that the method is most sensitive to surface cracking (primarily oriented in the longitudinal direction in this case) rather than to microcracking in the core. The lack of correlation between the energy transmission (SWT) and deterioration may be a result of the presence of an extensive cracking pattern on the specimen surfaces. This method was developed to determine the depth of one surface breaking crack, and other researchers have found that reflections off nearby cracks tend to interfere with the surface wave of interest for analysis [20].

4.3 Prism Samples

The observed expansions of the prism samples were in accordance with those measured in the beam specimens. The lack of expansion in the nonreactive prisms is further evidence that this concrete mixture was conducive to deterioration. Larger and more rapid expansions were measured in the prism samples corresponding to the second reactive beam due to the curing temperature difference, as discussed previously.

As with UPV and impact echo testing, the resonant frequency method is most useful at low levels of deterioration. As expansions increased, the dynamic elastic modulus became less sensitive to further deterioration. Additionally, it is very difficult to perform this method on structures, which have complex geometry, loads, and boundary conditions that complicate the relationship between resonant frequency and the dynamic elastic modulus. Thus, resonant frequency testing requires taking a core, which is semi-destructive, although is almost always done when evaluating a deteriorated structure.

5 CONCLUSIONS

Regarding the use of the five NDT methods investigated in this study for the evaluation of structures affected by ASR, the general conclusions of this study are summarized as follows:

- The compression wave velocity, as measured through UPV or impact echo testing, yields the most consistent and reliable trends. This velocity is most sensitive to increasing deterioration at low levels of expansion. As deterioration progressed, losses in velocity were less pronounced.
- The surface wave velocity (SASW) and energy transmission (SWT) yielded poor correlations with deterioration. The wide scatter of data in the SASW results and the essentially constant trend of the SWT results imply that these methods are not as useful for characterizing deterioration.
- The dynamic elastic modulus calculated from resonant frequency testing showed clear, consistent trends with expansion that are very similar to those in the compression wave velocity results. However, this method can only be performed on small samples and requires taking a core.
- None of the NDT methods investigated in this study have more potential than current testing and monitoring techniques to accurately predict structural behavior. Losses in compression wave velocity and dynamic elastic modulus indicate a reduction in stiffness with increasing deterioration, which is not observed in structural testing of large reinforced elements.

Finally, one important factor to consider when evaluating structures using NDT is the importance of a baseline measurement, or the value of the parameter being measured before deterioration occurred. This is especially important when measuring the compression wave velocity, as this parameter can vary from around 3700 to 5000 m/s in sound concrete depending on the 28-day compressive strength, concrete composition and the moisture saturation, among other factors [24,25]. A baseline velocity can be estimated from knowledge of the concrete composition and 28-day compressive strength, or from measurements on seemingly undamaged portions of the structure, but this estimation can bring about more uncertainty and error when interpreting the results.

6 REFERENCES

[1] The Institute of Structural Engineers (1992): Structural effects of alkali-silica reaction. London: SETO

[2] Clark, LA (1989): Critical review of the structural implications of the alkali silica reaction in concrete. Contractor Report 169, Transport and Road Research Laboratory, Crowthorne, Berkshire, United Kingdom.

[3] Bungey, JH (1991): Ultrasonic testing to identify alkali-silica reaction in concrete. British Journal of NDT (33-5): 227-231.

[4] Bach, F, Thorsen, T, and Nielsen, M (1992): Load carrying capacity of structural members subjected to alkali-silica reactions. 9th International Conference on Alkali-Aggregate Reaction in Concrete: 9-21. London: Concrete Society.

[5] Chana, PS, and Korobokis, GA (1992): The structural performance of reinforced concrete affected by alkali silica reaction: Phase II. Contractor Report 311, Transport and Road Research Laboratory, Crowthorne, Berkshire, United Kingdom.

[6] Ahmed, T, Burley, E, and Rigden, S (1998): The static and fatigue strength of reinforced concrete beams affected by alkali-silica reaction. ACI Materials Journal (95-4): 376-388.

[7] Fan, S and Hanson, JM (1998): Effect of alkali silica reaction expansion and cracking on structural behavior of reinforced concrete beams. ACI Structural Journal (95-5): 498-505.

[8] Monette, L, Gardner, J, and Grattan-Bellow, P (2000): Structural effects of the alkali-silica reaction on non-loaded and loaded reinforced concrete beams. 11th International Conference on Alkali-Aggregate Reaction: 999-1008. Quebec: Centre de Recherche Interuniversitaire sur le Béton

[9] Blight, GE, Alexander, MG, Schutte, WK, and Ralph, TK (1983): The effect of alkali-aggregate reaction on the strength and deformation of a reinforced concrete structure. 6th International Conference on Alkali-Aggregate Reaction: 401-410. Copenhagen: Technical University of Denmark.

[10] Imai, H, Yamasaki, T, Maehara, H, and Miyagawa, T (1983): The deterioration by alkali-silica reaction of Hanshin Expressway concrete structures – Investigation and repair. 6th International Conference on Alkali-Aggregate Reaction: 131-135. Copenhagen: Technical University of Denmark.
[11] Boenig, A (2000): Bridges with premature concrete deterioration: Field observations and large-scale testing. MS Thesis, The University of Texas at Austin, Austin, Texas, USA.
[12] Deschenes, D (2009): ASR/DEF damaged bent caps: Shear tests and field implications. MS Thesis, The University of Texas at Austin, Austin, Texas, USA.
[13] Larson, N (2010): Structural performance of ASR/DEF damaged prestressed concrete trapezoidal box beams with dapped ends. MS Thesis, The University of Texas at Austin, Austin, Texas, USA.
[14] Kreitman, K (2011): Nondestructive evaluation of reinforced concrete structures affected by alkali-silica reaction and delayed ettringite formation. MS Thesis, The University of Texas at Austin, Austin, Texas, USA.
[15] Bauer, S, Cornell, B, Figurski, D, Ley, T, Miralles, J, and Folliard, K (2006): Alkali-silica reaction and delayed ettringite formation in concrete: A literature review. Report No 0-4085-1, Center for Transportation Research, The University of Texas at Austin, Austin, Texas, USA.
[16] ASTM C1293 (2008): Standard test method for determination of length change of concrete due to alkali-silica reaction. American Society for Testing & Materials, West Conshoshocken.
[17] ASTM C597 (2009): Standard test method for pulse velocity through concrete. American Society for Testing and Materials, West Conshoshocken.
[18] ASTM C1383 (2004): Standard test method for measuring the P-wave speed and the thickness of concrete plates using the impact-echo method. American Society for Testing and Materials, West Coshoshocken.
[19] Sansalone, MJ, and Streett, WB (1997): Impact-Echo: Non-Destructive Evaluation of Concrete and Masonry. Jersey Shore: Bullbrier Press.
[20] Kee, S, and Zhu, J (2010): Using air-coupled sensors to determine the depth of a surface-breaking crack in concrete. The Journal of the Acoustical Society of America (127-3): 1279-1287.
[21] Zhu, J (2005): Non-contact NDT of concrete structures using air-coupled sensors. PhD Dissertation, University of Illinois at Urbana-Champaign.
[22] ASTM C215 (2008): Standard test method for fundamental transverse, longitudinal and torsional resonant frequencies of concrete specimens. American Society for Testing & Materials, West Conshoshocken.
[23] Corinaldesi, V, and Moriconi, G (2008): Alkali-aggregate reaction: From prognosis to intervention. 13th International Conference on Alkali-Aggregate Reaction. Trondheim: CD-ROM.
[24] Malhotra, VM, and Carino, NJ (2004): Handbook on Nondestructive Testing of Concrete. 2nd edition. CRC Press, West Conshoshocken.
[25] Ravindrarajah, RS, Khan, AS, and Pathmasiri, M (2002): Properties of high-strength high-performance concrete for marine environment. International Conference on Concrete in Marine Environment: 1-10. Hanoi: IABSE Vietnam National Center for Natural Science and Technology.

TABLE 1: Concrete Mixture Details for the Reactive and Nonreactive Beam Specimens.

Material	Amount	Reactive Mixture Materials	Nonreactive Mixture Materials
Cement	415 kg/m^3	Type III High-Alkali Cement from Lehigh Cement Company, Fleetwood, PA	Type III Low-Alkali Cement from Alamo Cement Company, San Antonio, TX
Water	237 kg/m^3	Hot Tap Water (about 55°C)	Cold Tap Water
Fine Aggregate	691 kg/m^3	Jobe-Newman Sand from Cemex, El Paso, TX	Colorado River Sand from Texas Concrete Materials, Del Valle, TX
Coarse Aggregate	890 kg/m^3	19 mm Crushed Limestone from Texas Crushed Stone Company, Georgetown, TX	19 mm Crushed Limestone from Texas Crushed Stone Company, Georgetown, TX
Sodium Hydroxide	40 kg/m^3 (reactive only)	50% NaOH Solution from Fisher Scientific Company, Pittsburgh, PA	---

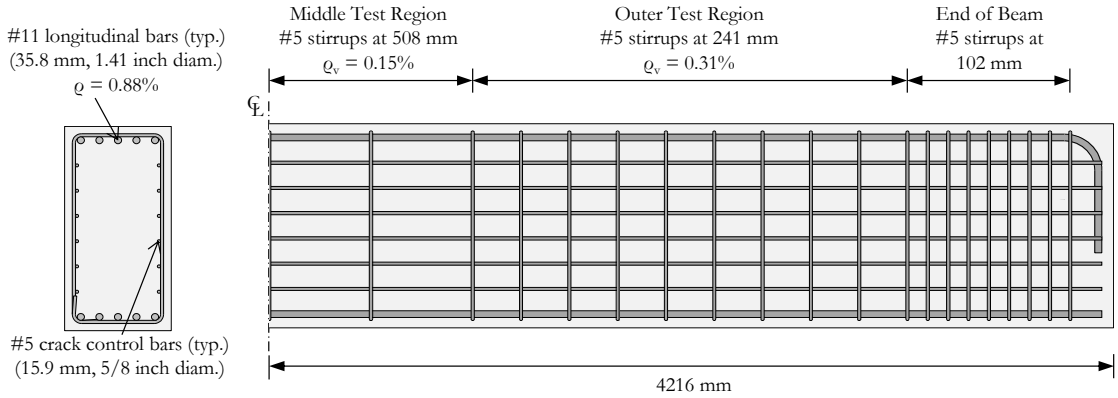

FIGURE 1: Geometry and reinforcement layout of the beam specimens. Note that the specimens are symmetric about the center line shown.

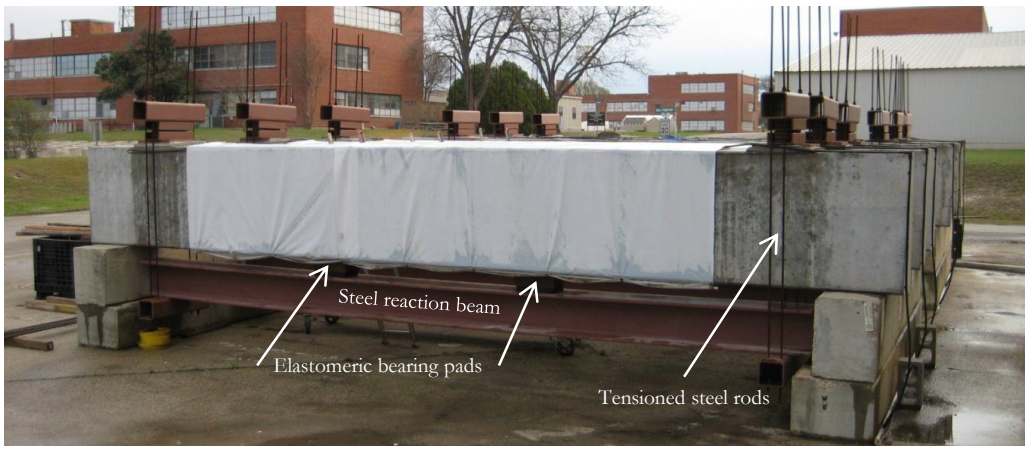

FIGURE 2: Specimens conditioning outdoors. Note the tarp wrapped around the specimens to trap in the moisture. The steel beam, tubes and rods are used to apply the simulated service load.

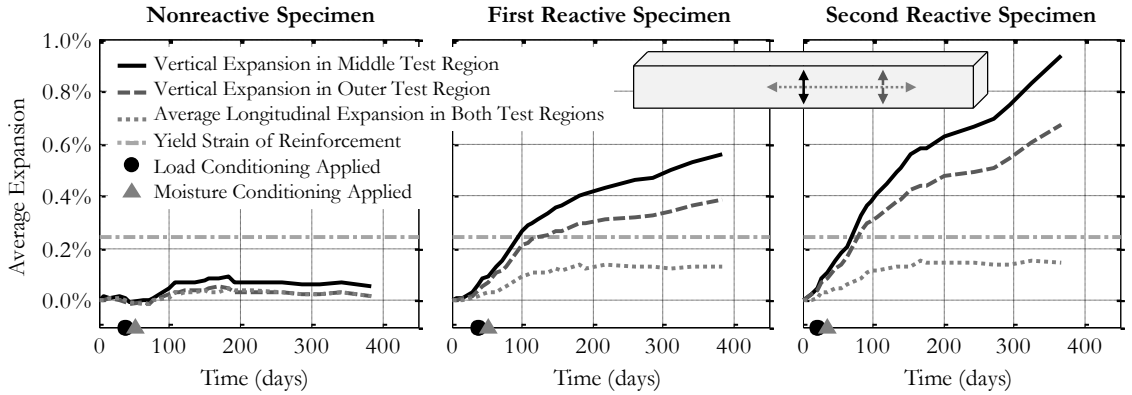

FIGURE 3: Results from expansion monitoring of the three beam specimens. The largest and most rapid expansions were observed in the vertical direction in the middle test region, where the reinforcement provides the least amount of restraint. The larger and more rapid expansions observed in the second reactive specimen are expected to be a result of the higher curing temperatures in this specimen.

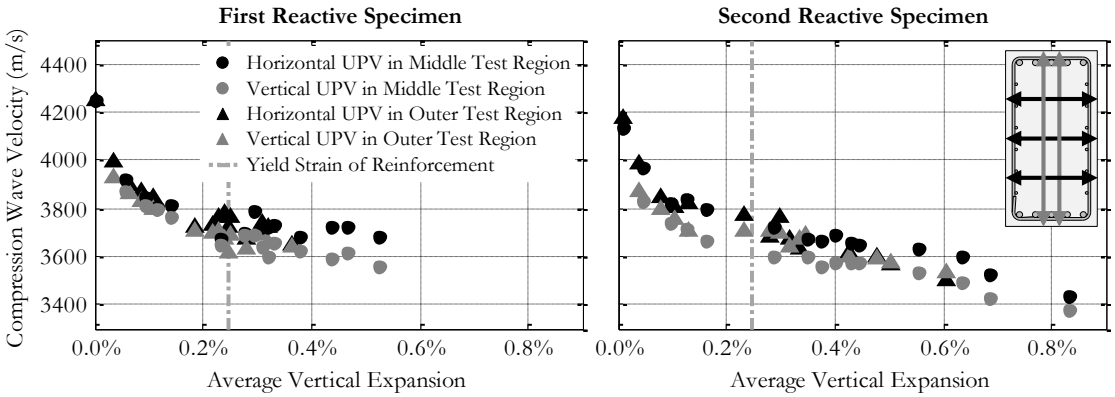

FIGURE 4: Results from UPV testing on the two reactive beam specimens. The compression wave velocity in the nonreactive specimen varied between 4225 and 4370 m/s over the monitoring period.

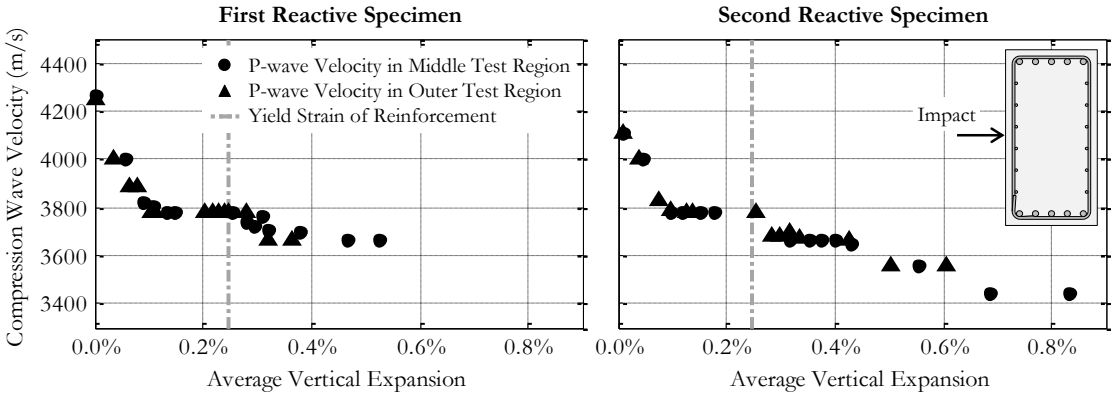

FIGURE 5: Results from impact echo testing on the two reactive beam specimens. The compression wave velocity in the nonreactive specimen varied between 4220 and 4390 m/s over the monitoring period.

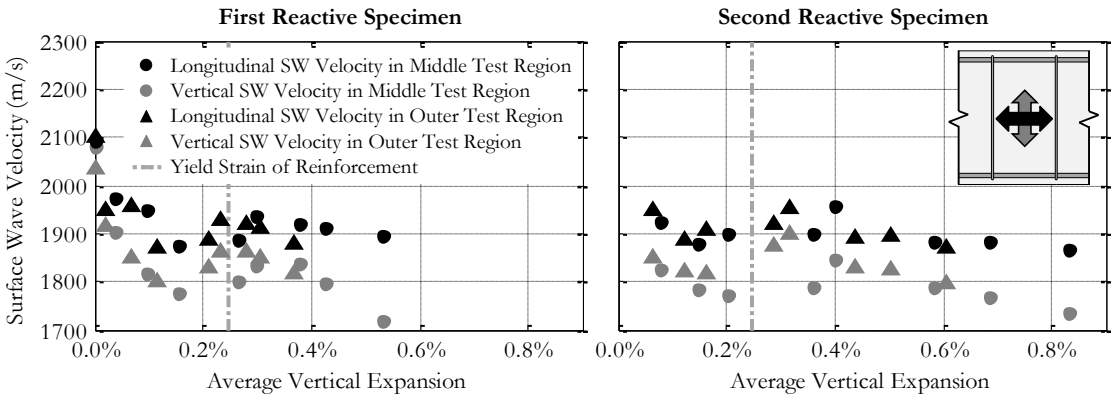

FIGURE 6: Results from SASW testing on the two reactive beam specimens. The surface wave velocity in the nonreactive specimen varied between 2020 and 2150 m/s over the monitoring period.

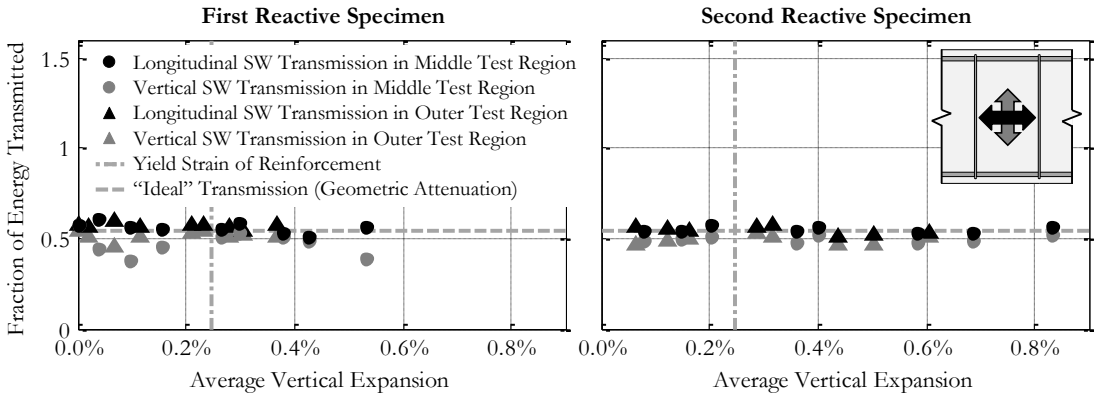

FIGURE 7: Results from SWT testing on the two reactive beam specimens. The fraction of SW energy transmission in the nonreactive specimen varied between 0.523 and 0.566 over the monitoring period. The "ideal" transmission includes only geometric attenuation of the point source-induced wave.

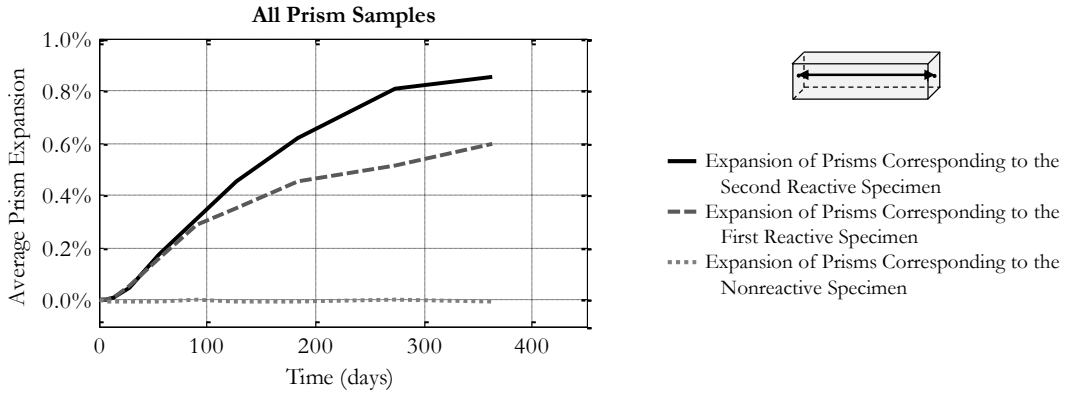

FIGURE 8: Results from expansion monitoring of the small prism samples cast alongside the large beam specimens. As with the beam specimens, larger and more rapid expansion was observed in the prisms corresponding to the second reactive specimen. This is likely due to higher curing temperatures.

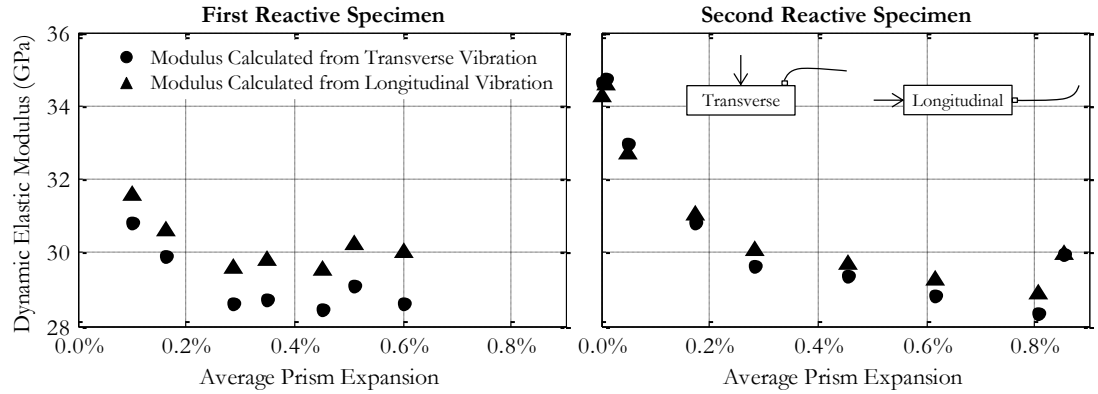

FIGURE 9: Results from resonant frequency testing of the reactive prism samples corresponding to the two reactive beam specimens. The dynamic modulus computed from the transverse and longitudinal vibration of the nonreactive prisms varied between 36.2 and 37.2 GPa over the monitoring period.